RadioGraphics

AAPM/RSNA Physics Tutorial for Residents: Topics in US

Beyond the Basics: Elasticity Imaging with US[1]

Timothy J. Hall, PhD

Editor's Note.— Although this article is based on information presented as part of the AAPM/RSNA Physics Tutorial for Residents at the 2002 RSNA scientific assembly, as the title suggests, it discusses a new technology not found in clinical practice and not typically covered in physics courses for residents. However, since this technology is very likely to be in clinical use in the near future, many readers should find this article interesting and timely.

A new mode of imaging with ultrasonography (US) is under development in several laboratories around the world. This technique allows estimation of some measure of the viscoelastic properties of tissue. The information displayed in the images is a surrogate for that obtained with manual palpation. Fundamental concepts in elasticity imaging include stress, strain, and the elastic modulus; strain imaging has received the most attention from researchers. A system for elasticity imaging is under development that produces images of mechanical strain in real time by means of a freehand scanning technique. This system is integrated into a clinical US system without any external equipment and involves software changes only. Data obtained with this system demonstrate that the relative stiffness of many fibroadenomas changes as they and the surrounding tissue are deformed. At elasticity imaging of in vivo breast lesions, invasive ductal carcinomas appear, on average, more than twice as large on the elasticity image than on the B-mode image, but fibroadenomas and cysts are nearly equal in size on the two image types. The usefulness of this technology and the new information it provides suggest that it might soon be available on commercial US systems.

Abbreviations: RF = radiofrequency, 1D = one-dimensional, 2D = two-dimensional, 3D = three-dimensional

Index terms: Breast neoplasms, diagnosis, 00.30 • Physics • Ultrasound (US), elastography, 00.12989 • Ultrasound (US), tissue characterization, 00.12989

RadioGraphics 2003; 23:1657–1671 • **Published online** 10.1148/rg.236035163

[1]From the Department of Medical Physics, University of Wisconsin, 1530 Medical Sciences Center, 1300 University Ave, Madison, WI 53706-1532. From the AAPM/RSNA Physics Tutorial at the 2002 RSNA scientific assembly. Received July 11, 2003; revision requested July 30 and received August 7; accepted August 14. Supported by grant DAMD17-00-1-0596 from the U.S. Army Medical Research and Materiel Command; supported in part by a research agreement with Siemens Medical Solutions, Ultrasound Group (Issaquah, Wash). **Address correspondence to** the author (e-mail: *tjhall@wisc.edu*).

Introduction

It is the experience of many that palpation, pressing on the surface of soft tissue in an effort to "feel" abnormalities, is a commonly used diagnostic tool. This tool has been used for thousands of years and is the primary diagnostic tool for some diseases. Examples include breast self-examination for sensing breast "lumps" and digital rectal examination for prostate cancer. Palpation is known to be subjective, and it lacks sensitivity to small abnormalities that are deep beneath the skin surface.

Improving sensitivity and reducing the subjectivity of palpation could have a significant impact on breast cancer prognosis. Breast cancer is the second-leading cause of cancer deaths in women. Over 200,000 new cases of invasive breast cancer are expected in the United States this year alone. It is anticipated that approximately 40,000 women in the United States will die of breast cancer in 2003. The prognosis for breast cancer patients is best when the disease is detected at an early stage. Specifically, 5- and 10-year survival statistics are best when cancer is noninvasive (1) and is less than 1 cm in diameter (2). Improvements in mammography have resulted in improved detection of breast lesions, and mammography can allow detection of smaller tumors in young women than either breast self-examination or clinical breast examination (3). However, mammography is not infallible. Approximately 15% of palpable breast cancers are not detectable with mammography, and this number is likely higher in younger women (4). A combination of clinical palpation with either mammography or ultrasonography (US) has been shown to significantly increase the sensitivity and specificity of breast cancer detection (5).

One of the greatest difficulties in mammography is imaging the radiographically dense breast. Unfortunately, women with mammographically dense breasts have a risk of breast cancer that is 1.8–6.0 times greater than that of women the same age with little or no mammographic density (6). Small lesions become much more difficult to detect when obscured by dense connective tissues and ducts. Several recent studies have demonstrated that US has higher sensitivity for breast cancer detection than mammography alone (7), mammography combined with physical examination (7,8), or mammoscintigraphy (9). Furthermore, the sensitivity of mammography decreases significantly with increasing mammographic density (7,10). Hormone replacement therapy reduces the sensitivity of x-ray mammography (11) and increases the need for alternate diagnostic tools.

In an effort to improve the sensitivity of palpation and provide quantitative measures of "palpable," research groups around the world are actively working toward imaging technologies that display quantitative maps of "tissue stiffness." This article reviews the physics of palpation and uses that information to describe the limitations of palpation. That basic physical understanding is then used to describe the various approaches to these imaging technologies. The emphasis then turns to elasticity imaging systems and the development of an elasticity imaging system that is implemented on a commercial US system and displays real-time elasticity images with freehand scanning. Results of preliminary tests of the usefulness of that system for diagnosing breast abnormalities are then described.

Previous reviews of elasticity imaging with US are available (12,13). This article updates those prior reviews and emphasizes a specific real-time elasticity imaging system and results obtained with that system.

Physics of Palpation

An understanding of how palpation works can be obtained by examining the basic physics of applying an external deformation to an object. Begin with a simple model of forces and deformation. A standard concept presented in introductory physics is the elastic deformation of a simple spring (a one-dimensional [1D] object) due to a known

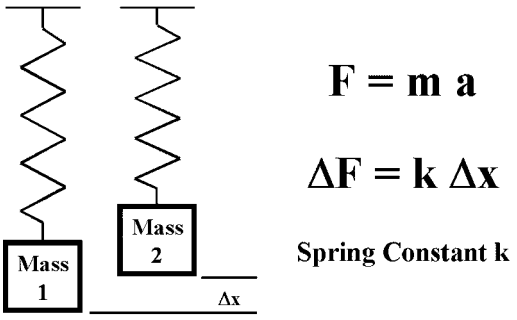

Figure 1. Introductory mechanics describes the behavior of a spring supporting different masses. Diagram shows how one spring would be stretched to two different lengths by two different masses. Hooke's law describes this behavior and can be used to characterize the spring under small deformations. Newton's second law equates a force, F, with a mass, m, and an acceleration, a. A known mass suspended from a spring exerts a known force due to the acceleration of gravity. Hooke's law relates the difference in the stretch of the spring, Δx, due to the change of force, ΔF, resulting from suspending different masses. The proportionality constant, k, characterizes the stiffness of the spring.

applied force. Figure 1 illustrates the typical simple experiment to study elasticity. A known mass suspended from a simple spring results in a measurable elongation of that spring. Suspending a different known mass results in a different elongation of the spring. Each mass in the standard gravitational field of the earth places a known force on the spring. The difference in these forces and the difference in the elongations of the spring due to those forces can be combined by using Hooke's law to estimate the spring constant, k, which is characteristic of the spring and quantifies its "stiffness."

To extend the concept of force and deformation to a three-dimensional (3D) object, consider separately the forces and resulting displacements. The analysis will be simplified by assuming that the material is homogeneous and isotropic (meaning that the material properties are uniform in composition without any directional dependence in elasticity). Ignore the class of forces, called *body forces*, that act on all volume elements of the material (such as gravity and inertia). The class of forces to consider are called *surface forces* because they have units of force per unit area and can be viewed as acting on a surface element of the object. That surface element is not necessarily on the exterior boundary of the object, but can be a surface of an arbitrary interior volume element.

The orientation of that surface is described by a vector that is perpendicular to the surface element (a normal vector); thus, a 3D coordinate system (x_i, $i = 1, 2, 3$ or x_1, x_2, x_3) is required to describe the normal vector. A force acting on that surface element has a magnitude and direction (force is a vector quantity), and the direction of that force is not necessarily perpendicular to the surface element. Thus, to describe the direction of the force vector also requires a 3D coordinate system (y_j, $j = 1, 2, 3$). To maintain generality and simplicity (to obtain principle components) in the description of the surface force, two separate 3D coordinate systems are used (x_i and y_j). Collapsing the arbitrary surface element to a point, we obtain a "stress tensor." A tensor is a generalization of the concept of a vector; tensor calculus is used to study the derivatives of vector fields. The stress tensor, σ_{ij}, is a 3×3 matrix corresponding to the nine combinations available by combining the two independent 3D coordinate systems of the force and the surface element on which it acts.

Similarly, consider the displacement of a volume element acted on by an external force. If the motion does not involve a change of volume or shape of the object, the motion is termed *rigid body motion*. On the other hand, if the object is deformed (changes shape or volume) as a result of the external force, the description of motion is again more complex. A 3D coordinate system is required to describe the motion in space. To maintain generality and simplicity (to obtain principle components) in the description of the gradients (spatial rate of change) of that deformation (strain is the spatial rate of change of displacement), another 3D coordinate system is required. The strain tensor, ϵ_{kl}, is thus another 3×3 matrix corresponding to the nine combinations available by combining these two independent 3D coordinate systems.

An equation to relate the nine-component stress tensor to the nine-component strain tensor is called a *constitutive equation*. The form of the constitutive equation depends on whether a material is a fluid (an ideal fluid with no viscosity or a

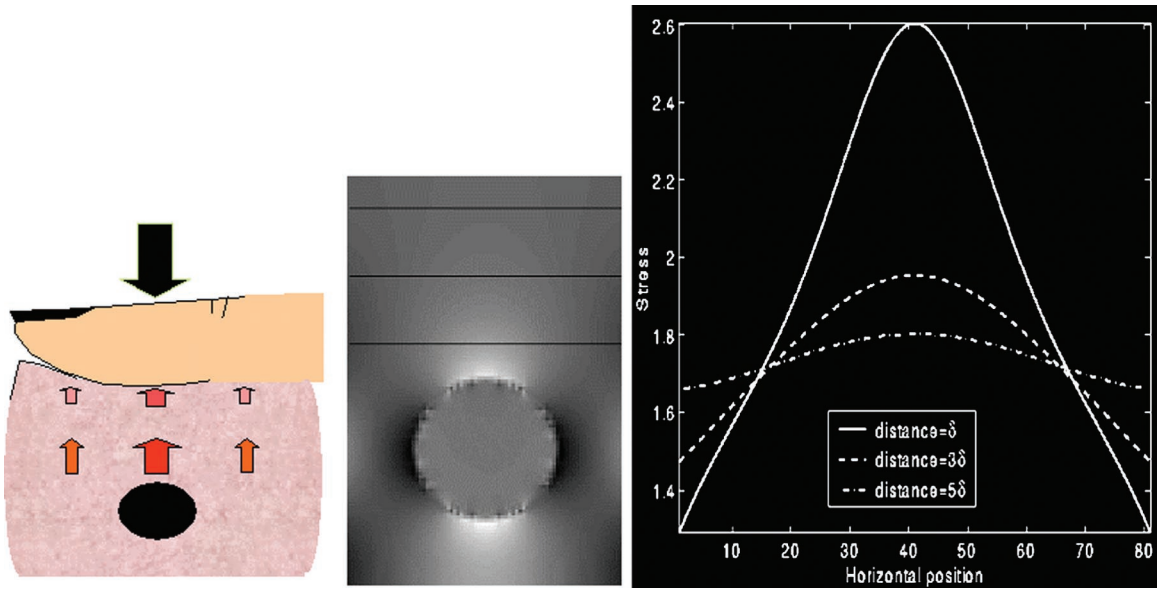

Figure 2. Palpation can be approximated with a simulation tool (finite element analysis). Left: Drawing shows uniform displacement of the top surface of a block containing a spherical object. Center: Image shows the axial stress distribution resulting from the displacement. Right: Plot shows profiles of the stress distribution across the lines in the center image. A large variation in the stress profile is seen for the profile close to the spherical object. This situation simulates location of the sphere near the surface of the block. As the profile moves further away from the sphere, the variation in stress across the profile decreases, suggesting that the sphere would be more difficult to palpate as it is placed deeper in the block.

Newtonian viscous fluid), purely elastic (eg, an idealized solid), or viscoelastic (neither purely viscous nor purely elastic). In a purely elastic (lossless) deformation, the stress is dependent only on the strain: $\sigma_{ij} = C_{ijkl}\,\epsilon_{kl}$. This equation is analogous to Hooke's law for the 1D spring, but it accounts for forces and deformations in all three directions.

The quantity C_{ijkl} is the "modulus tensor" of elastic coefficients and is the equivalent of the spring constant, k, used to describe the deformation of a spring. The four subscripts indicate that four sets of 3D coordinate systems are required for a general description of the relationship between the stress and strain tensors, and thus, C_{ijkl} has (3^4) 81 components. The stress and strain tensors are symmetric and therefore each contains at most six independent components. Therefore, the modulus tensor for infinitesimal elastic deformations is also symmetric and contains at most 36 independent components. By assuming a material to be completely isotropic, it can be shown (14) that the number of independent elastic coefficients is reduced to two (called the *Lamé constants*). A more detailed description of stress and strain can be found in any text on continuum mechanics (eg, reference 15).

The elastic coefficients that describe the behavior of a material are absolute measures of intrinsic properties of the material. Estimating these quantities requires measurements of stresses and strains under well-characterized experimental conditions. For example, the viscoelastic properties of many soft tissues under cyclic uniaxial loading are found to depend on the strain range, strain rate, measurement temperature, and so on (16). It is often easier to simplify the experiment and measure only components of the surface stress distribution or the internal strain distribution. The drawback is that stress or strain alone is a relative quantity and not intrinsic to the material under study.

The basic physics of elasticity (stress and strain) can be used to understand the limitations of palpation. Engineers often use a computational tool called *finite element analysis* to study the behavior of objects under external forces or deformations. Finite element analysis was used to simulate the stress and strain involved when deforming a uniform block containing a spherical inclusion (Fig 2). The upper surface of the block is uniformly displaced by 1% of the total height. The lower surface is allowed to move freely laterally, and the sides have unrestricted motion. Figure 2 shows the distribution of stress and profiles of that stress distribution. In palpation, the fingers press on the tissue to deform it and then sense the

Elastic Moduli of in Vitro Breast Tissue at Two Different Strain Ranges and Strain Rates

	Elastic Moduli by Strain Range and Strain Rate	
Type of Breast Tissue	5% Precompression, 10%/sec Strain Rate	20% Precompression, 20%/sec Strain Rate
Normal fat	19 ± 7	20 ± 6
Normal glandular tissue	33 ± 11	57 ± 19
Fibrous tissue	107 ± 32	233 ± 59
Ductal carcinoma in situ	25 ± 4	301 ± 58
Invasive ductal carcinoma	93 ± 33	490 ± 112

Note.—Ductal carcinoma demonstrates the largest difference between modulus measurements under these two conditions. This result suggests that it has the most nonlinear stress-strain relationship among the tissues studied.

stress distribution that results. The simulation shows that as the sphere moves further away from the surface (profile further from the sphere), the variation in stress across the profile decreases, suggesting that the sphere would be more difficult to palpate (less stress contrast available to the fingers to sense) as it is placed deeper in the block.

In Vitro Tissue Studies

The most common approach to studying the viscoelastic properties of soft tissues is to sinusoidally deform in vitro samples of tissue, measure the force required to induce the deformation, and study the phase relationship between force and displacement. In vitro studies of the viscoelastic properties of breast tissue (13,17) have demonstrated several findings that are significant to elasticity imaging (Table). First, for cyclic load-unload experiments, there is little phase delay between the sinusoidal deformation and response (strain and stress) for compression frequencies near 1 Hz. This shows that the energy required to deform the tissue is nearly completely recovered when the deforming force is released (nearly lossless deformation). Thus, in vitro breast tissue behaves as a nearly completely elastic medium at these strain rates, and the viscous component can be ignored. These deformation motion frequencies are typical of that used in clinical US breast examinations with compression.

Second, the stress-strain relationship for most breast tissues is nonlinear, and the degree of nonlinearity varies with tissue type. (Materials with linear stress-strain relationships exhibit stress that is directly proportional to strain; that is, they exhibit constant stiffness. Materials with nonlinear stress-strain relationships change stiffness, most commonly getting stiffer, as they are deformed.) Third, the elastic moduli of breast tissue, obtained from the slope of the stress-strain curves, vary significantly among breast tissue types and strain range. In summary, breast tissue is mostly elastic for the strain rates likely encountered with freehand scanning, object contrast is likely high in strain and modulus images, contrast will likely be different for different lesion types, and contrast will likely change with increasing compression.

Imaging the Elastic Properties of Tissue

Approaches to elasticity imaging can be classified by the modality of the signal source (primarily US or magnetic resonance [MR] imaging), the mechanical parameter estimated (eg, stress, strain, or modulus), or a descriptor of the experimental procedure ("dynamic" or "[quasi-]static" techniques). The mechanical properties estimated with these techniques are related. As described earlier, stress and strain are mutually responsive quantities, but they are not intrinsic material properties. Images of stress and strain are maps of a parameter relative to its surroundings (as a mammogram maps the relative x-ray attenuation, for example). Elastic moduli are intrinsic material properties generally described with a matrix (as described earlier), but for practicality experimental conditions are manipulated and material properties (such as incompressibility, homogeneity,

and isotropy) are assumed so that the size of this matrix is reduced to one or two parameters.

Several research groups are developing techniques for imaging the stress distribution. Most notable among the stress imaging techniques is the work from Wellman et al (18), who use a piezoresistive sensor array (Tekscan, Boston, Mass) coupled to a position-tracking system. This system closely mimics the mechanics of palpation and demonstrates a strong correlation between the size of the lesion measured with the tactile system and the lesion size measured following resection. The performance for small lesions (<10 mm) that are relatively deep (>10 mm) remains to be seen. Also noteworthy is the work of Sarvazyan (19), in which he attempts to solve the inverse problem of determining the 3D modulus distribution that causes the measured surface pressure distribution.

Strain imaging has received the most attention in elasticity imaging. The earliest implementations used M-mode acquisition and cross-correlation to track tissue motion and study tissue elasticity (20,21). In later studies, Doppler processing techniques were used to track differences in motion (22,23), and "sonoelasticity imaging" soon followed (24). The Doppler processing techniques were the first "dynamic techniques" and derived their data from US. "Static compression elastography" is the most common approach to strain imaging. Numerous groups are pursuing US-based strain imaging, with efforts in algorithm development (25–29), performance evaluation (30–32), and clinical testing (33,34) (representative citations).

The basic information derived in strain imaging techniques is the relative tissue displacement. An imaging system (typically US or MR imaging) acquires (predeformation) data corresponding to a map of tissue anatomy. A small deformation is applied, either through an external compressor or physiologic function (breathing, cardiac pressure variations, etc), and another (postdeformation) map of the anatomy is acquired. The displacement field in the deformed tissue is estimated by comparing these two maps of anatomy. Mechanical strain is estimated by calculating the gradient (the spatial rate of change) of the displacement field. In US, the displacement along the acoustic beam propagation (axial) direction can be estimated far more accurately and with higher precision than that in the lateral or elevational direction (32).

An important aspect for clinical acceptance of US strain imaging is the technique for deforming the soft tissue between image pairs. Most phantom experiments in the literature used motorized compression devices and extensive fixtures. These devices are not likely to gain clinical acceptance because they either limit the locations where strain imaging can be applied or are time-consuming to incorporate. Freehand scanning, in which tissue is deformed with the surface of the transducer, is desirable (33–35).

Developing a real-time strain imaging system that allows freehand scanning is essential for clinical usability. The strain imaging algorithm must be computationally efficient, be insensitive to motion irregularities, and track tissue motion in two dimensions (eventually three and four dimensions). Block-matching (template-matching) algorithms are widely used in image processing applications for tracking motion. The most notable application is movie image compression algorithms such as the Moving Picture Experts Group (MPEG) format. The use of block matching in US was initially reported by Trahey et al (36) for blood flow estimation. Block matching is a good candidate since it is simple in principle and is capable of tracking motion in two dimensions. However, for strain imaging, the algorithm needs to be modified to increase its computational efficiency and insensitivity to decorrelation noise (29). (Decorrelation is a measure of how similar two signals are. That similarity is measured with cross-correlation or surrogate measures of correlation. Echo signals decorrelate when there is high electronic noise or when there is large deformation of the tissue.)

There has been less attention focused toward strain imaging systems than toward strain imaging algorithms, data simulation, and performance testing. Doyley et al (35) have reported their progress in freehand elasticity imaging. Their system lacked real-time feedback in the data acquisition process; nevertheless, they found that it is possible to obtain good elasticity data with freehand scanning. Their rate of success was relatively low, and significant pre- and postprocessing were necessary to obtain accurate displacement estimates.

The system reported by Garra et al (33) used a modified mammography paddle with a hole cut out to provide an acoustic window. This allowed (relatively) easy correlation with the mammogram. However, the acoustic data acquisition system was crude. The system allowed scanning with only a 5-MHz transducer—lower than the standard of its day (7.5 MHz)—and had significantly

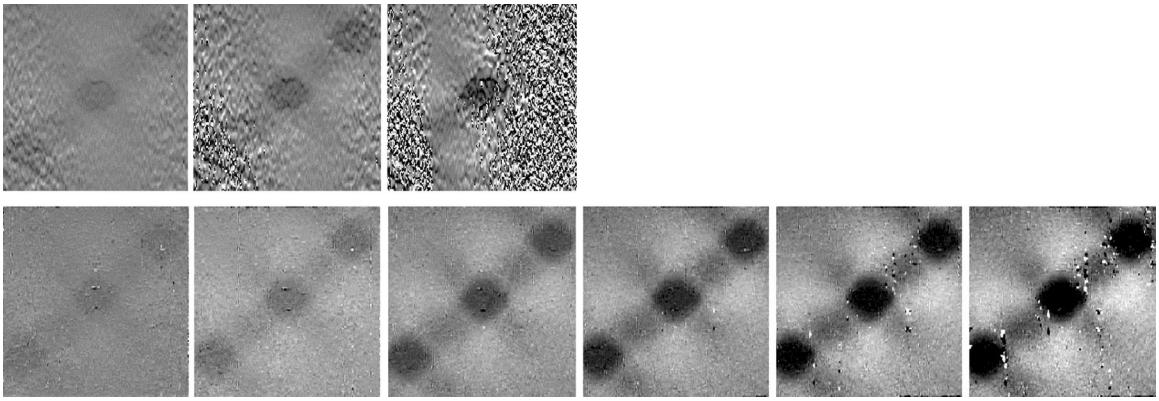

Figure 3. Images of the mechanical strain in the axial direction for a gelatin phantom with three cylinders that are three times stiffer than the background. Top row: Strain images obtained with 1D tracking by using cross-correlation. Bottom row: Strain images obtained with 2D companding (2D motion tracking). The applied deformation (top and bottom rows) from left to right is 0.6%, 1.2%, 2.4%, 3.6%, 4.8%, and 6.0% strain. With 1D tracking (top row), lateral expansion (bulging) occurring with axial compression causes the echo A-lines to not match and the echo signals to decorrelate. Two-dimensional tracking (bottom row) is able to track the lateral as well as axial motion to allow acquisition of strain images with a higher contrast-to-noise ratio.

poorer performance than current systems. In addition, the digitization was external to the US scanner, resulting in reduced electronic signal-to-noise ratio and increased timing jitter in the acquired echo signals. The increased jitter significantly reduces the performance of displacement estimates in strain imaging. The current system used by that group incorporates a midrange US scanner with a five-axis motor controlled compression system (37). The first real-time elasticity imaging system was developed for prostate imaging (38). Data were acquired in a sector-shaped scan from an endocavity transducer, and a 1D tracking method was used. As a result, elasticity image frame rates were quite high at the expense of image quality.

The in vivo studies of strain imaging reported by Garra et al (33) demonstrated that strain imaging has merit in differentiating among solid tumors in breasts. Their most significant finding was that invasive ductal carcinomas are significantly wider in strain images than in the corresponding B-mode image. This difference is likely due to the desmoplastic reaction that surrounds this tumor type.

Modulus imaging has also been investigated, and there are three primary approaches in the literature. The first approach estimates the shear wavelength in tissue and from this directly estimates the shear modulus of the tissue (39–41). The other techniques require simultaneous measurements of stress and strain and require assumptions regarding the boundary conditions of the experiment (42–46). Compared with strain imaging, modulus imaging has lower spatial resolution and higher noise, and the assumptions regarding boundary conditions can result in biased estimates. However, estimating an intrinsic tissue parameter, instead of the relative parameters estimated in stress or strain images, makes this an attractive approach.

There are also methods under development that use acoustic radiation force to deform tissue and study tissue viscoelasticity (47–49) with promising results. Other novel approaches to describing the viscoelastic behavior of tissues, such as those reported by Fatemi et al (50,51), are also under investigation.

Early work in strain imaging demonstrated the limitations of tracking motion in one dimension and motivated the development of two-dimensional (2D) and 3D motion-tracking algorithms for elasticity imaging (27,28,52). Those studies demonstrated that 1D tracking failed to correctly track motion in a 3-cm-wide field of view with as little as 0.6% compression, and motion-tracking errors became increasingly worse with increased compression. However, by using 2D tracking algorithms that appropriately compensate for lateral motion, high contrast-to-noise images of mechanical strain could be obtained with compressions of more than 5% in phantoms (Fig 3). The basic approach, called *companding*, was to use 2D motion tracking to align (warp) either the pre- or postdeformation data field prior to 1D cross-correlation.

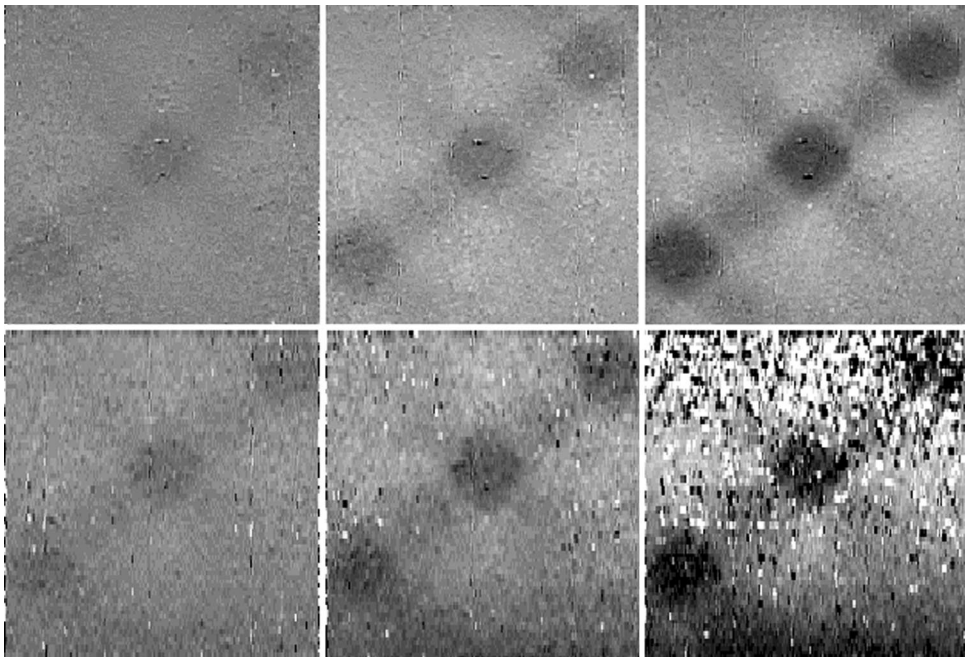

Figure 4. Images of a gelatin phantom with varying deformation (from left to right, 0.6%, 1.2%, and 2.4% axial strain). Top row: Images acquired with the top and bottom surfaces slipping freely and with minimal elevational motion, as in Figure 3. Bottom row: Images acquired near the edge (in elevation, perpendicular to the image plane) of the phantom, which was bound in elevation at the bottom and slid freely at the top. As the phantom was deformed, the top slid out of the image plane in elevation, resulting in decorrelation of the echo signals. Increasing the deformation caused greater decorrelation.

Other early work also demonstrated the need to control motion during elasticity imaging experiments. The images in Figure 4 demonstrate that it is essential to control the motion during deformation, especially with regard to elevation motion. A typical clinical US system acquires echo data, nominally, from a plane of tissue. Any out-of-plane motion of tissue will result in echo signal decorrelation and reduced elasticity image quality.

The key to obtaining high-quality elasticity images is the quality of the motion-tracking algorithm. Ultrasound radiofrequency (RF) echo signals, the same data used to form a B-mode image, are used as a map of anatomy. Those same signals are used to track the deformation of the anatomy. The task is to accurately track the anatomic deformation with minimal uncertainty (displacement estimate variance or covariance). A review of many of the techniques used for tracking tissue motion with ultrasound can be found in reference 53. A tutorial on the general topic of waveform coherence and time-delay estimation can be found in reference 54.

A review of the assumptions used in signal correlation analysis can help one appreciate the difference between many motion-tracking algorithms. A typical assumption in motion tracking based on the time delay of ultrasound echo signals is that the deformation of the tissue is minimal (or recoverable) within the echo signal segment being tracked. Another common assumption is that the observation window (data segment length) is large compared to the time delay. Thus, a relatively long data segment is needed to avoid ambiguous displacement estimates (referred to as *peak hopping*). The plot in Figure 5 demonstrates that with an RF echo segment as short as 3 mm and with only 1.5% axial strain, there is obvious echo signal decorrelation between the pre- and postdeformation A-lines. However, the single

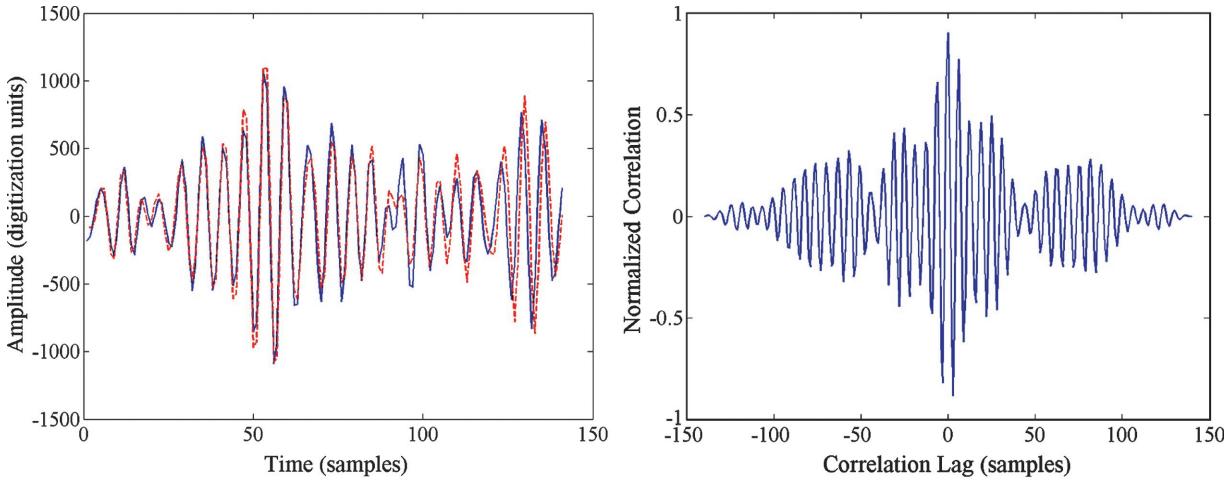

Figure 5. **(a)** Plot of the predeformation (red dashed line) and postdeformation (solid blue line) data for a 3-mm segment (140 RF samples) of the echo signals from the center of a gelatin phantom under 1.5% axial strain. The postdeformation signal has been shifted in time to match the predeformation signal as closely as possible. The deformation has caused decorrelation in the echo signals, which reduces coherence (cross-correlation coefficient = 0.87). **(b)** Plot of the cross-correlation function comparing the predeformation and time-delayed postdeformation RF echo signals. The single large positive peak suggests that there is little ambiguity in the correct delay required to match these signals.

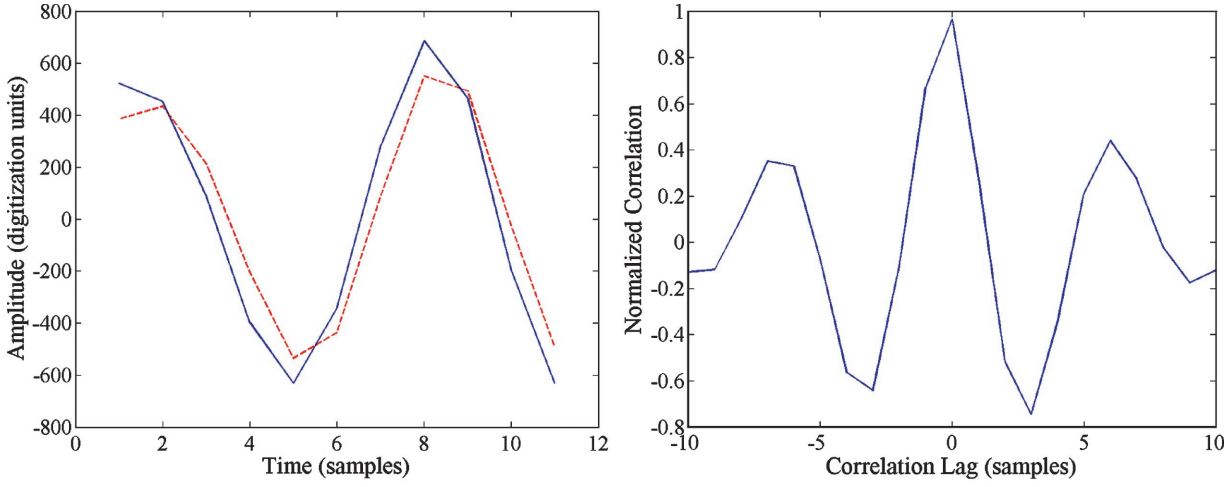

Figure 6. **(a)** Plot of the predeformation (red dashed line) and postdeformation (solid blue line) data for a 0.24-mm segment (11 RF samples) of the echo signals from the center of a gelatin phantom under 1.5% axial strain. The postdeformation signal has been shifted in time to match the predeformation signal as closely as possible. Little decorrelation in the echo signals within this short echo segment results in high coherence (cross-correlation coefficient = 0.96). **(b)** Plot of the cross-correlation function comparing the predeformation and time-delayed postdeformation RF echo signals.

large peak in the cross-correlation function plotted in Figure 5 demonstrates that there is little ambiguity in the time delay required to match pre- and postdeformation signals.

Use of shorter RF echo segments in motion tracking reduces the decorrelation within the echo signal segment and increases the waveform coherence (Fig 6). However, short data segments increase the likelihood of time-delay ambiguity (eg,

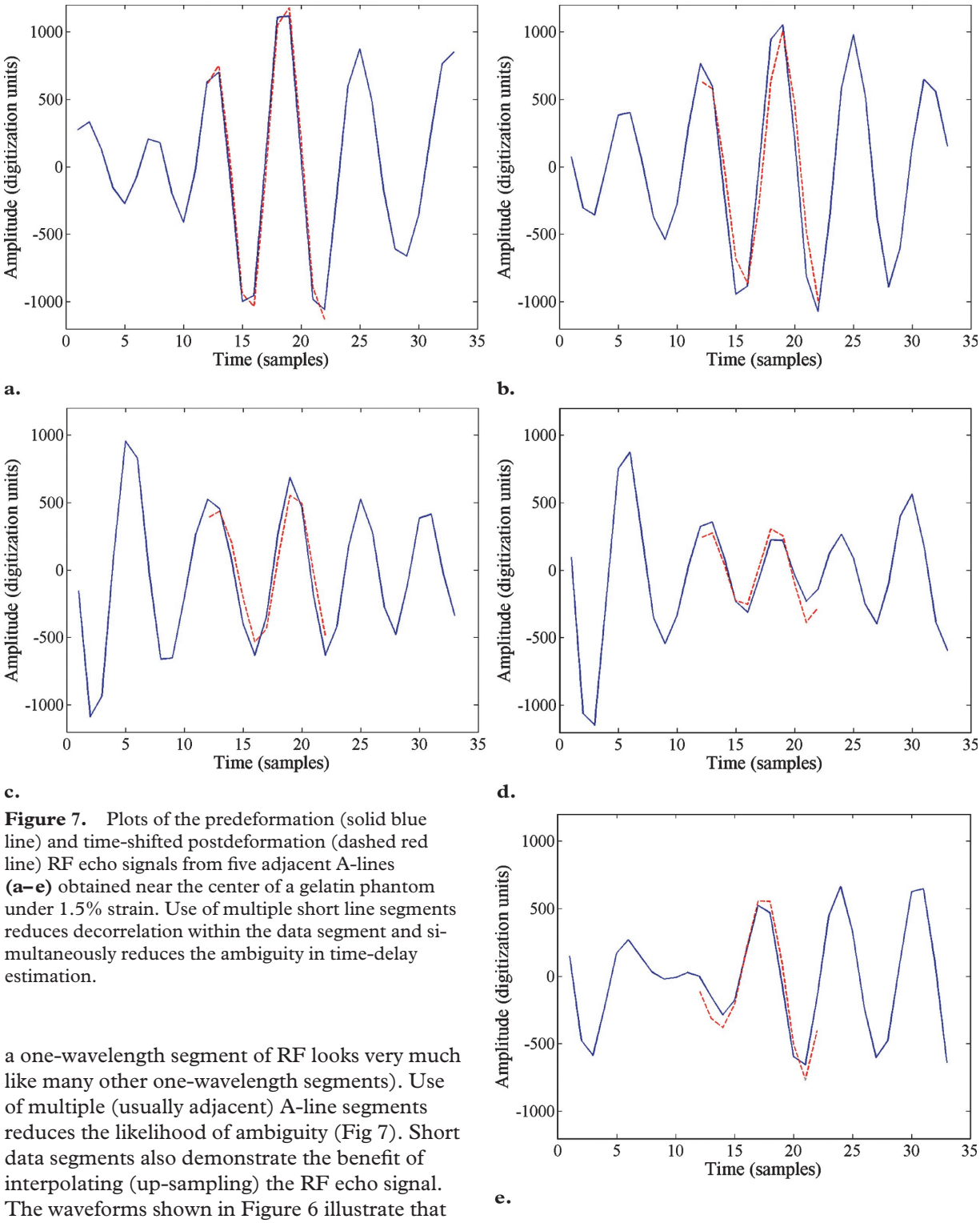

Figure 7. Plots of the predeformation (solid blue line) and time-shifted postdeformation (dashed red line) RF echo signals from five adjacent A-lines **(a–e)** obtained near the center of a gelatin phantom under 1.5% strain. Use of multiple short line segments reduces decorrelation within the data segment and simultaneously reduces the ambiguity in time-delay estimation.

a one-wavelength segment of RF looks very much like many other one-wavelength segments). Use of multiple (usually adjacent) A-line segments reduces the likelihood of ambiguity (Fig 7). Short data segments also demonstrate the benefit of interpolating (up-sampling) the RF echo signal. The waveforms shown in Figure 6 illustrate that waveform coherence would improve if time delays of less than one sample were available. An alternative is to interpolate the correlation function, but this requires a model for the functional form of the cross-correlation function. If up-sampling the RF echo signal can be justified, it reduces the need for an accurate model of the cross-correlation function when interpolating subsample displacement estimates (Fig 8).

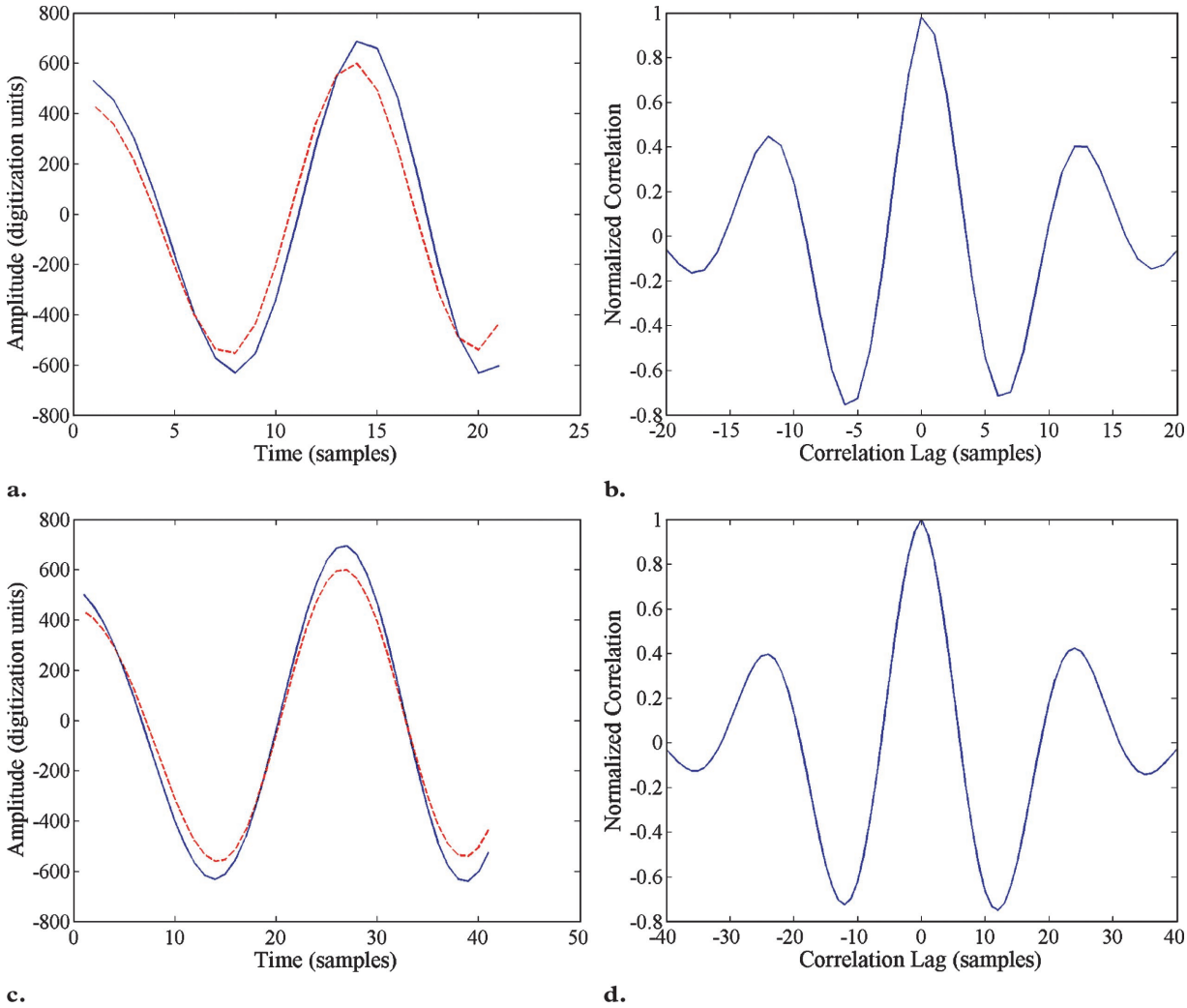

Figure 8. Plots of the predeformation (red dashed line in **a** and **c**) and postdeformation (solid blue line in **a** and **c**) data for a 0.24-mm segment of the echo signals at 1.5% axial strain acquired at a 36-MHz sampling frequency upsampled to 72 MHz **(a, b)** and 144 MHz **(c, d)**. The postdeformation signal has been shifted in time to match the predeformation signal as closely as possible. As the effective sampling interval is reduced, the integer time-delay error is also reduced, allowing greater waveform coherence. (Correlation coefficients of 0.965 [Fig 6], 0.978, and 0.998 were obtained with 36-MHz, 72-MHz, and 144-MHz sampling, respectively.)

Development of a Real-Time Strain Imaging System

Experience in developing motion-tracking algorithms and experiments with phantoms and in vitro tissues suggest criteria for a clinically viable elasticity imaging system. First, the system must track tissue motion in two dimensions (or three dimensions, if available) for high contrast-to-noise images (27,28). Second, the system should use short 2D data segments (kernels) for motion tracking to minimize decorrelation within the data segments and to minimize time-delay ambiguity. Third, the system should provide real-time elasticity images, as well as normal B-mode images, to allow the user to monitor the images being acquired and manipulate the transducer array with freehand scanning, thus ensuring that the tissue motion is suitable for forming high-quality elasticity images. In addition, the data acquisition technique should be similar to that currently used in US to increase the likelihood of clinical acceptance. A large deviation from standard clinical practice would likely receive a more skeptical assessment by potential users than a subtle modification to current practice.

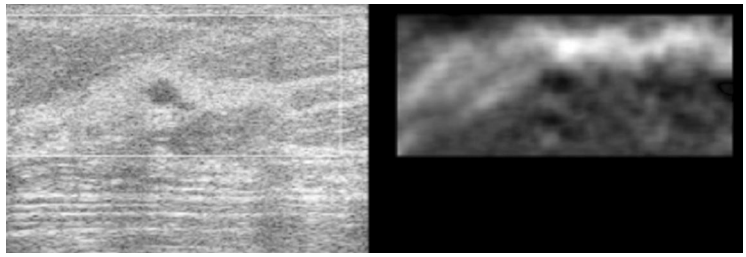

Figure 9. B-mode (left) and elasticity (mechanical strain) (right) images of an in vivo breast cyst 3 mm in diameter show that small in vivo structures are resolvable on strain images.

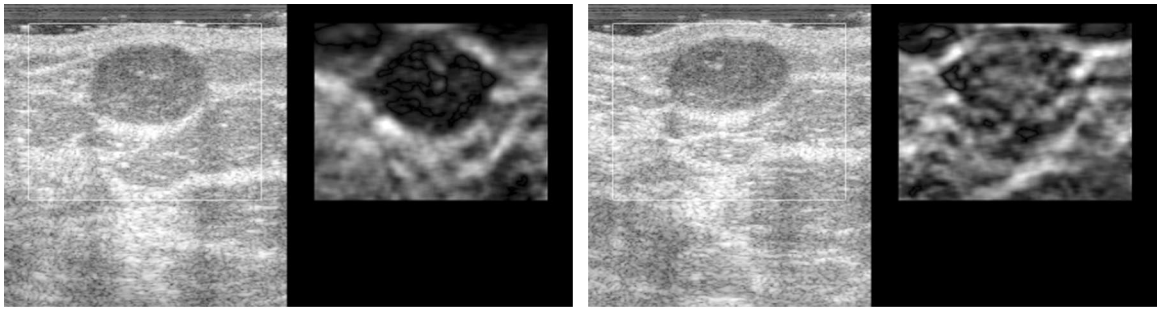

a. **b.**

Figure 10. B-mode (left) and strain (right) images of a typical fibroadenoma under different amounts of preload (deformation): low preload **(a)** and increased preload **(b)**. For both elasticity images, the average strain is about 1.2%. The images obtained at low preload **(a)** were acquired with the US transducer just barely in contact with the skin surface. At low preload, fibroadenomas are typically stiff relative to the surrounding glandular tissue. As the preload increases **(b)**, the contrast of the fibroadenoma on the strain image decreases and the stiffness of the lesion appears nearly equal to that of the surrounding tissue.

A novel motion-tracking algorithm has been developed and implemented on a clinical US system (Sonoline Elegra; Siemens Medical Solutions, Issaquah, Wash) (29). Phase-sensitive (I-Q) echo data are processed internally in real time on this system to estimate displacement and strain. The system can use any of the linear-array transducers available on the Elegra and is compatible with tissue harmonic imaging on that system. The system displays B-mode and strain images side by side on the normal system display at about seven frames per second. A region of interest (ROI) is displayed in the B-mode image, and displacement and strain are estimated for tissue within that ROI. The size and location of the ROI can be manipulated with front panel controls. When scanning, the normal freeze and cine capabilities of the system are available. When a sequence of data is acquired and stored (frozen), online postprocessing capabilities allow the ROI location and size to be modified, and other common tools such as modifying the gray-scale mapping are available. Initial tests of the elasticity image noise and spatial resolution are found in reference 29. Spherical lesions as small as 2.4 mm in diameter that are three times stiffer than the background were easily displayed. The protocol for clinical testing of this system was approved by the Humans Subjects Committee at the University of Kansas Medical Center, where that initial work was performed.

A critical issue in the development and use of any imaging system is the achievable spatial resolution for a given task. The ability to image a 3-mm-diameter sphere in a phantom is encouraging. More important, those encouraging results are corroborated by the ability to image small structures in vivo. For example, images of an in vivo 3-mm cyst are shown in Figure 9. Although the ability to image small structures in vivo is clearly demonstrated, the required contrast to view objects of a specific size is unknown. Investigations are under way to evaluate this through contrast-detail analysis (55).

The ability to acquire and view long sequences of elasticity images has provided the opportunity to observe nonlinear elastic behavior of in vivo tissues. Nonlinearity in the stress-strain relationship of tissue was observed with in vitro breast tissues (17) and was therefore expected with in vivo tissues, but it was only recently observed with the availability of a real-time elasticity imaging system (34). Figure 10 shows an example of

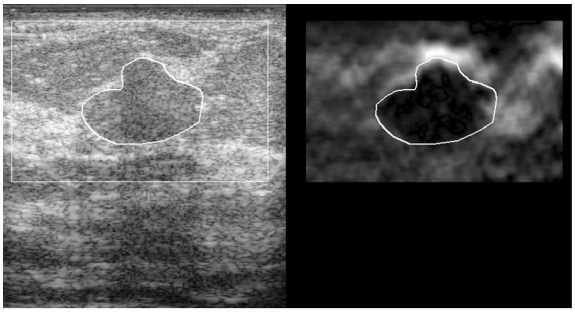

11.

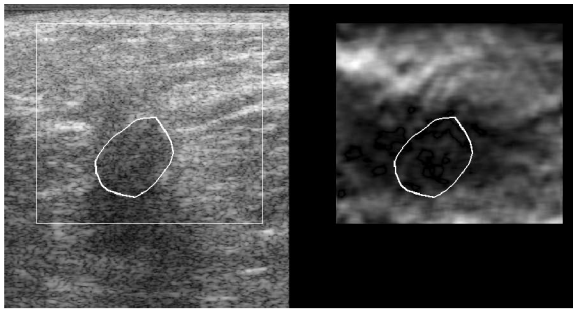

12.

Figures 11, 12. **(11)** B-mode (left) and strain (right) images of a fibroadenoma. The lesion is traced on the B-mode image, and that tracing is displayed on the strain image. The size and shape of the lesion on the two images are very similar. **(12)** B-mode (left) and strain (right) images of a scirrhous invasive ductal carcinoma. The lesion is traced on the B-mode image, and that tracing is displayed on the strain image. The lesion is larger on the strain image (right) than on the B-mode image (left).

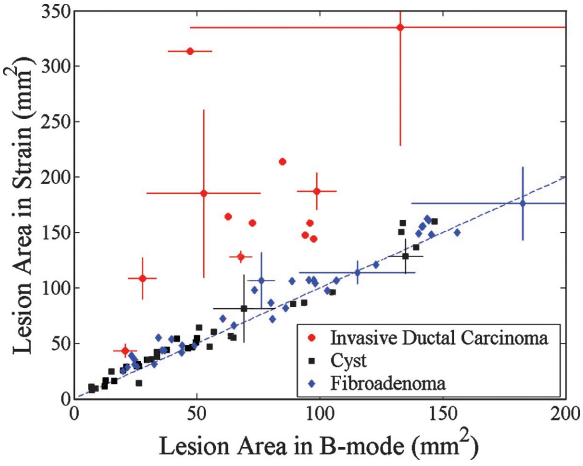

Figure 13. Plot of lesion area measured on strain images versus on corresponding B-mode images for cysts, fibroadenomas, and invasive ductal carcinomas. The average results of five observers are plotted. Dashed line = equal area on both image types, error bars = standard deviations of the measurements.

the implications of nonlinear elasticity in strain imaging. At low preload (transducer barely in contact with the skin surface and minimal pressure applied), the fibroadenoma appears dark in the strain image. As the preload is increased (pressure applied with the transducer increasing deformation), the strain image contrast of the fibroadenoma (its stiffness relative to the surrounding tissue) decreases. This behavior might explain why others have found that some fibroadenomas are not visible in single strain images (33).

One of the significant findings in prior clinical trials of in vivo elasticity imaging (33) was that the size of a breast lesion displayed in strain images, relative to its size in a normal B-mode image, appears to be a significant criterion for differentiating malignant from benign breast lesions. Figures 11 and 12 show examples of the B-mode and strain image pairs for a fibroadenoma and an invasive ductal carcinoma, respectively. In each case, the lesion is traced in the B-mode image and that tracing is reproduced in the respective strain image. The lesion boundary traced for benign lesions has about the same size and shape in the two image types. However, the lesion boundary traced in B-mode images of invasive ductal carcinomas is much smaller than the lesion displayed in the respective strain image. On average, the area of these carcinomas displayed in strain images is three times larger than that in B-mode images (34). It is postulated (33,34) that the increased size of carcinomas in strain images is due to the desmoplasia that often surrounds invasive ductal carcinoma.

To test the usefulness of relative lesion size for differentiating between benign and malignant breast lesions, five observers individually viewed a set of image sequences from in vivo breast elasticity imaging. Each observer selected the image pair from a sequence (movie loop) that was most representative of the B-mode and strain image pair from that sequence. Each observer then traced the outline of the lesion in each image type and measured the width and height of the lesion in each image. This was repeated for data from 97 movie loops of 55 unique lesions in 29 patients. A plot of the average lesion area for each lesion measured by the group of observers is shown in Figure 13. These data are consistent with those reported by others (33) and suggest that elasticity imaging may be a helpful tool to improve the usefulness of breast US. If the ratio of lesion size in strain images versus in B-mode images proves to be a sensitive criterion for increasing confidence of a benign diagnosis, the fraction of biopsy specimens that prove to be benign tissue will likely be

reduced at significant savings in health care expense and trauma to patients and their families and friends.

Conclusions

Elasticity imaging is a relatively new technique for studying the stiffness of tissue. The information acquired with these techniques is similar to that obtained with manual palpation, but elasticity imaging is more sensitive and less subjective than palpation. Further, the information is provided in an image format so that it can be compared with data from other image modalities and can more easily be documented and shared with others.

Several interesting approaches to elasticity imaging are currently being investigated by research groups around the world. Different approaches provide different information about the viscoelastic properties of tissue. Many of these approaches emphasize the elastic properties of tissue due to the techniques of data acquisition.

At least one method for elasticity imaging is under development that produces images of mechanical strain in real time by using a freehand scanning technique very similar to that of standard breast US examinations. The system is integrated into a clinical US system without any external equipment and involves software changes only. In vivo tests of this system have demonstrated the ability to image small breast lesions with confidence. It has also allowed visualization of the effects of nonlinear elasticity of in vivo breast tissues. Further investigations with this system suggest that benign breast lesions are about the same size and shape in B-mode and strain images, but invasive ductal carcinomas tend to be significantly larger in strain images than in the corresponding B-mode images. This fact suggests that elasticity imaging might increase the usefulness of breast US and might be offered in clinical US systems in the near future.

Acknowledgments: The author is grateful to many for their contribution to this effort. Significant contributions came from Yanning Zhu, PhD, in algorithm development and implementation, Candace Spalding, RT, RDMS, RVT, for clinical coordination and assistance in developing elasticity scanning techniques, and Patrick Von Behren, PhD, for technical assistance and the loan of the US system used in this research.

References

1. Sariego J, Zrada S, Byrd M, Matsumoto T. Breast cancer in young patients. Am J Surg 1995; 170: 243–245.
2. Peer PG, Verbeek AL, Ravunac MM, et al. Prognosis of younger and older patients with early breast cancer. Br J Cancer 1996; 73:382–385.
3. McPherson CP, Swenson KK, Jolitz G, Murray CL. Survival among women ages 40–49 years with breast carcinoma according to method of detection. Cancer 1997; 79:1923–1932.
4. Costanza ME, Edmiston KL. Breast cancer screening: early recognition. Compr Ther 1997; 23:7–12.
5. Yang WT, Mok CO, King W, Tang A, Metreweli C. Role of high frequency ultrasonography in the evaluation of palpable breast masses in Chinese women: alternative to mammography? J Ultrasound Med 1996; 15:637–644.
6. Boyd NF, Dite GS, Stone J, et al. Heritability of mammographic density, a risk factor for breast cancer. N Engl J Med 2002; 347:886–894.
7. Hou MF, Chuang HY, Ou-Yang F, et al. Comparison of breast mammography, sonography and physical examination for screening women at high risk of breast cancer in Taiwan. Ultrasound Med Biol 2002; 28:415–420.
8. Kolb TM, Lichy J, Newhouse JH. Comparison of the performance of screening mammography, physical examination, and breast US and evaluation of factors that influence them: an analysis of 27,825 patient evaluations. Radiology 2002; 225: 165–175.
9. Wang HC, Chen DR, Kao CH, et al. Detecting breast cancer in mammographically dense breasts: comparing technetium-99m tetrofosmin mammoscintigraphy and ultrasonography. Cancer Invest 2002; 20:932–938.
10. Saarenmaa I, Salminen T, Geiger U, et al. The effect of age and density of the breast on the sensitivity of breast cancer diagnostic by mammography and ultrasonography. Breast Cancer Res Treat 2001; 67:117–123.
11. Laya MB, Larson EB, Taplin SH, et al. Effect of estrogen replacement therapy on the specificity and sensitivity of screening mammography. J Natl Cancer Inst 1996; 88:643–649.
12. Gao L, Parker KJ, Lerner RM, Levinson SF. Imaging of the elastic properties of tissue: a review. Ultrasound Med Biol 1996; 22:959–977.
13. Ophir J, Alam SK, Garra B, et al. Elastography: ultrasonic estimation and imaging of the elastic properties of tissues. Proc Inst Mech Eng H 1999; 213:203–233.
14. Tschoegl NW. The phenomenological theory of linear viscoelastic behavior: an introduction. New York, NY: Springer-Verlag, 1989.
15. Fung YC. A first course in continuum mechanics. Englewood Cliffs, NJ: Prentice Hall, 1994.
16. Fung YC. Biomechanics: mechanical properties of living tissues. 2nd ed. New York, NY: Springer-Verlag, 1993.
17. Krouskop TA, Wheeler TM, Kallel F, Garra BS, Hall T. Elastic moduli of breast and prostate tissues under compression. Ultrason Imaging 1998; 20:260–274.
18. Wellman PS, Dalton EP, Krag D, et al. Tactile imaging of breast masses: first clinical report. Arch Surg 2001; 136:204–208.
19. Sarvazyan A. Mechanical imaging: a new technology for medical diagnostics. Int J Med Inf 1998; 49:195–216.
20. Dickinson RJ, Hill CR. Measurement of soft tissue motion using correlation between A-scans. Ultrasound Med Biol 1982; 8:263–271.

21. Wilson LS, Robinson DE. Ultrasonic measurement of small displacements and deformations of tissue. Ultrason Imaging 1982; 4:71–82.
22. Krouskop TA, Dougherty DA, Vinson FS. A pulsed Doppler ultrasonic system for making noninvasive measurements of the mechanical properties of soft tissue. J Rehabil Res Dev 1987; 24:1–8.
23. Yamakoshi Y, Sato J, Sato T. Ultrasonic imaging of internal vibration of soft tissue under forced vibration. IEEE Trans Ultrason Ferroelectr Freq Control 1990; 37:45–53.
24. Lerner RM, Huang SR, Parker KJ. Sonoelasticity images derived from ultrasound signals in mechanically vibrated tissues. Ultrasound Med Biol 1990; 16:231–239.
25. Ophir J, Cespedes EI, Ponnekanti H, et al. Elastography: a quantitative method for imaging the elasticity of biological tissues. Ultrason Imaging 1991; 13:111–134.
26. O'Donnell M, Skovoroda A, Shapo B, Emelianov S. Internal displacement and strain imaging using ultrasonic speckle tracking. IEEE Trans Ultrason Ferroelectr Freq Control 1994; 41:314–325.
27. Chaturvedi P, Insana MF, Hall TJ. 2-D companding for noise reduction in strain imaging. IEEE Trans Ultrason Ferroelectr Freq Control 1998; 45:179–191.
28. Insana MF, Chaturvedi P, Hall TJ, Bilgen M. 3-D companding using linear arrays for improved strain imaging. In: Proceedings of the 1997 IEEE Ultrasonics Symposium. New York, NY: Institute of Electrical and Electronics Engineers, 1997; 1435–1438.
29. Zhu Y, Hall TJ. A modified block matching method for real-time freehand strain imaging. Ultrason Imaging 2002; 24:161–176.
30. Bilgen M, Insana MF. Elastostatics of a spherical inclusion in homogeneous biological media. Phys Med Biol 1998; 43:1–20.
31. Bilgen M, Insana MF. Deformation models and correlation analysis in elastography. J Acoust Soc Am 1996; 99:3212–3224.
32. Insana MF, Cook LT, Bilgen M, Chaturvedi P, Zhu Y. Maximum-likelihood approach to strain imaging using ultrasound. J Acoust Soc Am 2000; 107:1421–1434.
33. Garra BS, Cespedes EI, Ophir J, et al. Elastography of breast lesions: initial clinical results. Radiology 1997; 202:79–86.
34. Hall TJ, Zhu Y, Spalding CS. In vivo real-time freehand palpation imaging. Ultrasound Med Biol 2003; 29:427–435.
35. Doyley M, Bamber JC, Fuechsel F, Bush NL. A freehand elastographic imaging approach for clinical breast imaging: system development and performance evaluation. Ultrasound Med Biol 2001; 27:1347–1357.
36. Trahey GE, Allison JW, von Ramm OT. Angle independent ultrasonic detection of blood flow. IEEE Trans Biomed Eng 1987; 34:965–967.
37. Merritt CR, Forsberg F, Liu J, Kallel F. In vivo elastography in animal models: feasibility studies (abstr). J Ultrasound Med 2002; 21:S98.
38. Lorenz A, Sommerfeld HJ, Garcia-Schurmann M, et al. A new system for the acquisition of ultrasonic multicompression strain images of the human prostate in vivo. IEEE Trans Ultrason Ferroelectr Freq Control 1999; 46:1147–1154.
39. Dutt V, Kinnick RR, Muthupillai R, Oliphant TE, Ehman RL, Greenleaf JF. Acoustic shear-wave imaging using echo ultrasound compared to magnetic resonance elastography. Ultrasound Med Biol 2000; 26:397–403.
40. Sandrin L, Tanter M, Catheline S, Fink M. Shear modulus imaging with 2-D transient elastography. IEEE Trans Ultrason Ferroelectr Freq Control 2002; 49:426–435.
41. Sandrin L, Tanter M, Gennisson JL, Catheline S, Fink M. Shear elasticity probe for soft tissues with 1-D transient elastography. IEEE Trans Ultrason Ferroelectr Freq Control 2002; 49:436–446.
42. Skovoroda AR, Emelianov SY, O'Donnell M. Tissue elasticity reconstruction based on ultrasonic displacement and strain images. IEEE Trans Ultrason Ferroelectr Freq Control 1995; 42:747–765.
43. Sumi C, Suzuki A, Nakayama K. Estimation of shear modulus distribution in soft-tissue from strain distribution. IEEE Trans Biomed Eng 1995; 42:193–202.
44. Kallel F, Bertrand M. Tissue elasticity reconstruction using linear perturbation method. IEEE Trans Med Imaging 1996; 15:299–313.
45. Doyley M, Meaney PM, Bamber JC. Evaluation of an iterative reconstruction method for quantitative elastography. Phys Med Biol 2000; 45:1521–1540.
46. Zhu Y, Hall TJ, Jiang J. A finite-element approach for Young's modulus reconstruction. IEEE Trans Med Imaging 2003; 22:890–901.
47. Nightingale KR, Palmeri ML, Nightingale RW, Trahey GE. On the feasibility of remote palpation using acoustic radiation force. J Acoust Soc Am 2001; 110:625–634.
48. Fatemi M, Greenleaf JF. Application of radiation force in noncontact measurement of the elastic parameters. Ultrason Imaging 1999; 21:147–154.
49. Tanter M, Bercoff J, Sandrin L, Fink M. Ultrafast compound imaging for 2-D motion vector estimation: application to transient elastography. IEEE Trans Ultrason Ferroelectr Freq Control 2002; 49:1363–1374.
50. Fatemi M, Greenleaf JF. Ultrasound-stimulated vibro-acoustic spectrography. Science 1998; 280: 82–85.
51. Fatemi M, Wold LE, Alizad A, Greenleaf JF. Vibro-acoustic tissue mammography. IEEE Trans Med Imaging 2002; 21:1–8.
52. Chaturvedi P, Insana MF, Hall TJ. Testing the limitations of 2-D companding for strain imaging using phantoms. IEEE Trans Ultrason Ferroelectr Freq Control 1998; 45:1022–1031.
53. Hein IA, O'Brien WD. Current time-domain methods for assessing tissue motion by analysis from reflected ultrasound echoes: a review. IEEE Trans Ultrason Ferroelectr Freq Control 1993; 40:84–102.
54. Carter GC. Coherence and time-delay estimation: an applied tutorial for research, development, test, and evaluation engineers. New York, NY: IEEE Press, 1993.
55. Madsen EL, Frank FR, Krouskop TA, et al. Low-contrast spherical lesion phantoms for assessing elastography performance (abstr). Ultrason Imaging 2003; 25:61.